

Journal of Materials Chemistry A

Accepted Manuscript



This is an *Accepted Manuscript*, which has been through the Royal Society of Chemistry peer review process and has been accepted for publication.

Accepted Manuscripts are published online shortly after acceptance, before technical editing, formatting and proof reading. Using this free service, authors can make their results available to the community, in citable form, before we publish the edited article. We will replace this *Accepted Manuscript* with the edited and formatted *Advance Article* as soon as it is available.

You can find more information about *Accepted Manuscripts* in the [Information for Authors](#).

Please note that technical editing may introduce minor changes to the text and/or graphics, which may alter content. The journal's standard [Terms & Conditions](#) and the [Ethical guidelines](#) still apply. In no event shall the Royal Society of Chemistry be held responsible for any errors or omissions in this *Accepted Manuscript* or any consequences arising from the use of any information it contains.

One-step Fabrication of Mixed-Halide Perovskite Film for High-efficiency Inverted Solar cell and Module

Chien-Hung Chiang^b, Jun-Wei Lin^a, Chun-Guey Wu^{a,b,*}

* ^{a,b} Professor: Chun Guey Wu, Master student: Chun-Wei Lin,
Department of Chemistry and Research Center for New Generation Photovoltaics,
National Central University, Jhong-Li, Taiwan 32001, ROC.
Fax: 886-3-4227664
E-mail: t610002@cc.ncu.edu.tw.

^b Research associate: Chien-Hung Chiang
Research Center for New Generation Photovoltaics,
National Central University, Jhong-Li, Taiwan 32001, ROC.

Organic-inorganic perovskite such as $\text{CH}_3\text{NH}_3\text{PbX}_3$ (X: halide) was proved to be a photo absorber for the solar cell since 2009.¹ The technique is then proceeding on an unprecedented trajectory: Within 6 years, the efficiency of perovskite solar cell increases to more than 19%²⁻⁴ and 22.1% efficiency was certified recently.⁵ Perovskite materials, besides the phenomenal efficiency of the corresponding cell, has the advantages of low cost, high absorption coefficient, excellent carrier transport rate (the carrier mobility which is up to $50 \text{ cm}^2/\text{V-s}$),⁶ all solid components⁷ and tunable compositions as well as can be fabricated by various non-expensive processings.⁸⁻¹³ The high-efficiency device reported generally has a small active area however to be commercially viable, up-scaling the device area is necessary. Several methods such as close space sublimation,¹⁴ air flow-assisted PbI_2 blade coating,¹⁵ and using a new lead precursor such as $\text{Pb}(\text{CH}_3\text{CO}_2)_2 \cdot 3\text{H}_2\text{O}$ ¹⁶ or additive¹⁷ had been used to prepare large area perovskite film. A module area of 100 cm^2 with efficiency of 4.3% was achieved.¹⁴

In the past several years, our group had developed a two-step spin-coating method to fabricate high quality perovskite films on PEDOT:PSS for the inverted perovskite solar cell.¹⁸⁻²⁰ In this paper we intend to develop a simple, reproducible and scalable method to fabricate large-area, high quality perovskite film for the inverted solar cell module by spin-coating using common precursors such as MAX and PbX_2 (X: halogen). Furthermore it was known that the halide in $\text{CH}_3\text{NH}_3\text{PbX}_3$ perovskite is a vital parameter in determining the intrinsic properties (such as electric, electronic and optical properties), film morphology and therefore the photovoltaic performance of the perovskite. For example both experimental results¹ and theoretical calculation data²¹ show that adding Cl in $\text{CH}_3\text{NH}_3\text{PbI}_3$ will not change the absorption onset ($\sim 800 \text{ nm}$) of perovskite but improve the film morphology.²² Furthermore $\text{CH}_3\text{NH}_3\text{PbCl}_3$ although having low stability, has a lower lying HOMO compared to $\text{CH}_3\text{NH}_3\text{PbI}_3$.

As a result $\text{CH}_3\text{NH}_3\text{PbI}_{3-x}\text{Cl}_x$ has a higher carrier lifetime and carrier transport rate than $\text{CH}_3\text{NH}_3\text{PbI}_3$ and also more stable than $\text{CH}_3\text{NH}_3\text{PbCl}_3$.^{3,11,23}

On the other hand, Cheng,²⁴ Noh,²⁵ and Jeon²⁶ *et al.* found that $\text{CH}_3\text{NH}_3\text{PbI}_{3-x}\text{Br}_x$ is more stable than $\text{CH}_3\text{NH}_3\text{PbI}_3$ film under the ambient atmosphere having moderate (>35%) humidity. In the presence of Br the distorted tetragonal of $\text{CH}_3\text{NH}_3\text{PbI}_3$ will turn to the more ordered cubic structure of $\text{CH}_3\text{NH}_3\text{PbBr}_3$, increasing the thermal stability.²⁷ $\text{CH}_3\text{NH}_3\text{PbBr}_3$ has higher LUMO and lower HOMO energy level²⁵ than $\text{CH}_3\text{NH}_3\text{PbI}_3$. Therefore solar cell based on $\text{CH}_3\text{NH}_3\text{PbBr}_3$ (or $\text{CH}_3\text{NH}_3\text{PbI}_x\text{Br}_{3-x}$) exhibit higher open-circuit voltage^{1,28,29} although the J_{sc} will be sacrificed. Moreover, the reported good quality perovskite films deposited on the mesoporous TiO_2 film (instead of compact TiO_2 layer) prepared with one-step solution process are generally containing more than one type of halogen.³⁰ In general mixed-halide perovskite film can be deposited on a flat substrate more facilely than full-halide perovskite (such as $\text{CH}_3\text{NH}_3\text{PbI}_3$ or $\text{CH}_3\text{NH}_3\text{PbBr}_3$) using one-step method, due to the former crystallizes slower therefore better quality film can be obtained. Therefore precursor solution containing three types of halogen was used for searching the simple film preparation conditions.

The objective of this study focused on developing a simple one-step (without anti-solvent treatment) method to fabricate good-quality perovskite films. Precursor solution with high concentration may be necessary for preparing good quality film. Therefore only PbI_2 , $\text{CH}_3\text{NH}_3\text{Cl}$, and $\text{CH}_3\text{NH}_3\text{Br}$ were used as starting materials for the mixed-halide perovskite, due to the low solubility of PbCl_2 and PbBr_2 in DMF. We first fixed the concentration of two components and changed the concentration of the other one to test the photovoltaic performance of the resulting mixed-halide perovskite films. The highest efficiency cells based on the films fabricated from the precursor solutions containing various stoichiometries of the halides are listed in

Table 1. When the mole ratio of $\text{CH}_3\text{NH}_3\text{Cl}$, $\text{CH}_3\text{NH}_3\text{Br}$ and PbI_2 in the precursor solution is 4:1:3, the corresponding device has the highest efficiency of 9.24%. We also test the photovoltaic performance of $\text{CH}_3\text{NH}_3\text{PbI}_3$ film prepared from 0.6 M ($\text{CH}_3\text{NH}_3\text{I} + \text{PbI}_2$)/DMF precursor solution using the same method and the efficiency of the resulting device is very low (<1%). Certainly the inverted cell based on $\text{CH}_3\text{NH}_3\text{PbI}_3$ film with the efficiency much higher than 10% is also possible by sophisticated/well-controlled fabrication process such as by hot-casting,³¹ (anti-)solvent washing,³² or two-step spin coating.¹⁹

To explore the compositions and structure of the mixed-halide perovskite films prepared from the precursor solutions with various amounts of the halides, EDS, GIXRD and UV/Vis absorption data were taken. The atomic ratio (listed in Table 2, estimated from the EDS data) of iodine and bromine in the films is closed to that in the precursor solution. For example the atomic ratios of I/Br is 6 and 3 in the precursor solutions, the corresponding films have the I/Br atomic ratio of 6.4 and 3.2, respectively. Nevertheless the content of chlorine in the film is much lower than that in the precursor solution (similar phenomenon was observed by Yang *et al.*³) even the film was made with a one-step spin-coating method. It may be due to the size of Cl^- ion (181 pm) is much smaller than that of I^- ion (220 pm). Chlorine ion may be too small to replace iodine in the lattice point of perovskite as proposed by Mosconi *et al.*³³ The source for Cl ($\text{CH}_3\text{NH}_3\text{Cl}$) or the resulting full-chlorine perovskite ($\text{CH}_3\text{NH}_3\text{PbCl}_3$) are very unstable, they may decompose to $\text{CH}_3\text{NH}_2(\text{g})$, $\text{HCl}(\text{g})$ (or PbCl_2) during the thermal annealing (100 °C) process.³⁴⁻³⁶ However, proper amount of Cl is necessary for preparing high performance mixed-halide film, when the amount of MACl decreases (from 4:1:3 to 3:1:3) or increases (from 4:1:3 to 5:1:3) in the precursor solution, the efficiency of the corresponding cells decreases as the data

displayed in Table 1.

The GIXRD spectra (Figure 1) of the mixed-halide perovskite films reveal that Film-1 (prepared with the precursor solution containing only MAI and PbI₂ with the formula of CH₃NH₃PbI_{2.4}Cl_{0.6}) has two diffraction peaks at 2θ lower than 15 degree, belong to PbI₂ (100) plane (12.25°) and CH₃NH₃PbI₃ (110) plane (13.8°),³⁷ respectively. No diffraction peak belongs to CH₃NH₃PbCl₃ or PbCl₂ was detected. Excess MAI did not react with all PbI₂ to form CH₃NH₃PbI_xCl_{3-x}, instead only CH₃NH₃PbI₃ and unreacted PbI₂ phases were detected in the XRD pattern. It was known³⁸ that the (110) diffraction of CH₃NH₃PbI₂Cl occurs at 14.10°. We did not observe any diffraction peak at 2θ between 14.10° and 13.8° for Film-1, may be due to that the Cl content is too low or Cl did not occupy the lattice point of perovskite. Cl in CH₃NH₃PbI_{2.4}Cl_{0.6} film may exist as small-sized PbCl₂ grain (XRD silent) which distributed randomly in CH₃NH₃PbI₃ film. Film-2 and Film-3 (both contain three types of halogen) show only one crystalline phase and their (110) and (220) diffraction peaks shift to higher angle, at the same time the crystalline domain size also increases slightly compared to those of CH₃NH₃PbI_{2.4}Cl_{0.6} film (Film-1). Moreover, the (110) diffraction peak of the Film-2 and Film-3 falls between 13.8° to 15.2° (15.2° is the diffraction angle of the (110) plane for CH₃NH₃PbBr₃,^{20,39,40}) and shifts to higher angle as Br content in the film increases. The XRD data suggest that Br atom may replace iodine in the lattice point of perovskite, due to the size of Br⁻ ion (196 pm) is not so different from that of I⁻ ion (220 pm). The same conclusion was made by Noh²⁵ *et al* in the preparation of CH₃NH₃PbI_{3-x}Br_x film which containing only I and Br in the precursor solution. Interestingly, the d-spacing of CH₃NH₃PbI_{3-x}Br_x (see Table 2) is not directly proportional to I/Br atomic ratio: such as the d-spacing of CH₃NH₃PbI_{3-x}Br_x is equal to 6.43 Å X (3-x)/3 + 5.83 Å X x/3. Nevertheless, the decreasing in the d-spacing by inserting Br in MAPbI₃ lattice seems has a

proportional to the Br content: for example compared to MAPbI₃ the d-spacing of CH₃NH₃PbI_{2.2}Br_{0.3}Cl_{0.5} is 0.05 Å smaller, whereas the d-spacing of CH₃NH₃PbI_{2.09}Br_{0.65}Cl_{0.26} is 0.11 Å smaller. Now we are trying to grow single crystals of CH₃NH₃PbI_{3-x}Br_x to study the relationship between the stoichiometry of I/Br and the d-spacing of CH₃NH₃PbI_{3-x}Br_x perovskite.

UV/Vis absorption spectra of the mixed-halide (Film-1 ~ 3) and full-iodide perovskite films are illustrated in Figure 2. CH₃NH₃PbI₃ has two local absorption maxima (λ_{\max}) at *ca.* 506 nm and 750 nm with an on-set absorption at 800 nm.¹⁸ The absorption on-set for CH₃NH₃PbBr₃ is 550 nm and the two λ_{\max} are at *ca.* 415 nm and 525 nm.²⁸ Two λ_{\max} for Film-1 are 484 nm and 750 nm which is slightly blue-shifted for the short wavelength peak but similar for the longer wavelength peak, respectively compared to those of CH₃NH₃PbI₃. This is a general phenomenon observed in the absorption spectra of CH₃NH₃PbI₃ and CH₃NH₃PbI_{3-x}Cl_x films.³⁸ On the other hand, both λ_{\max} values for Film-2 and Film-3 are all blue-shifted compared to those of Film-1 and CH₃NH₃PbI₃, consistency with the higher band gap (shorter λ_{\max}) of CH₃NH₃PbI_{3-x}Br_x. Film-3 with more Br content has shorter λ_{\max} compared to Film-2, which consists with the GIXRD data, implying that some iodine atoms in CH₃NH₃PbI₃ lattice were replaced by bromine atoms in the Film-2 and Film-3. Furthermore the shift in λ_{\max} can be an indication for the Br content in CH₃NH₃PbI_{3-x}Br_x film, just like the changes in the d-spacing obtained from the GIXRD patterns.

GIXRD patterns displayed in Figure 1 also show that the crystalline domain and crystallinity of the mixed-halide perovskite film increase as the content of Br in the film increases. Nevertheless, the efficiency of the cell based on Film-2 is higher than that for the device using Film-3 (with more Br content) active layer. The crystallinity and crystalline domain size of the active film may not be the only parameters for

determining the efficiency of a perovskite solar cell. It was known that the morphology of the active film also has a large impact on the photovoltaic performance of the perovskite solar cell. SEM images (both surface and cross-section) of Film-1 ~ 3 were taken and displayed in Figure 3. In the absence of Br, Film-1 is quite smooth however with a lot of holes/defects. The surface roughness of the Film-2 slightly higher than that of Film-1 however no hole was observed. Further increases the Br content of the film (Film-3), the surface roughness increases further, therefore the efficiency of the corresponding device decreases. Furthermore Film-1 containing no bromide is very fragile; the film frequently falls apart when it was broken-in-half to study the morphology of the cross-section. Therefore the cross-section image reveals lots of voids formed by loosely aggregated small particles, consistent with the fragile nature. On the other hand, the cross section of both Br-containing films (Film-2 and Film-3) is rather dense and shows a close contact to PEDOT:PSS layer. High roughness of Film-3 could be the major reason for the low efficiency.

In the composition screen process we found the stoichiometry of MACl/MABr/PbI₂ in the precursor solution for achieving the best efficiency is 4:1:3. The next screen step is to change the concentration of PbI₂ but keep the same mole ratio of the *three* components and the photovoltaic parameters of the resulting inverted cells are summarized in Table 3. The highest efficiency device was based on the film made from the precursor solution with the concentration of PbI₂/DMF equal to 0.6 M. However, when the concentration of PbI₂ is higher than 0.35 M the precursor solution may over-saturate at room temperature. When the precursor solution was passed through a 0.22 μm filter, precipitate was formed inside the filter. Therefore the fabrication of the devices should be controlled very precisely (such as the temperature and the standing time of the precursor solution) to obtain the reproducible results. However, the purpose of this study is to find a very simple method to prepare good

quality film for the inverted perovskite solar module. To simplify the fabrication process and obtain the reproducible results, 0.35 M precursor solutions were used. Perovskite film prepared from low precursor concentration with high spin rate is very thin, therefore, the spin program was optimized simultaneously and the photovoltaic performance of the corresponding films is also listed in Table 3. Data in Table 3 show that the best performance film was prepared from 0.35 M precursor solution using a consecutive one-step two-stage spin: 1000 RPM, 10 sec, then 7000 RPM, 20 sec. The highest power conversion efficiency is close 12% with the V_{oc} of 1.03 V (the I-V curve was illustrated in Figure S1, Electronic Supporting Information (ESI)) and quite reproducible as the efficiency statistics data also listed in Table 3.

Spin coating is a well-known technique for depositing thin film on a substrate. It is also a common technique used to prepare perovskite film for the inverted perovskite solar cells. The solution dripped on the substrate was applied with a centrifugal force, excess solution was spun-off, at the same time solvent in the film evaporates and dry film was formed on the substrate.²⁸ Perovskite film fabricated with one-step spin coating method involves a fast three dimensional crystallization reaction. Therefore sophisticatedly manipulating the solvent evaporation (therefore crystal growing) is necessary for obtaining continuous, fully coverage film on a smooth surface. To further improve the quality of perovskite film to enhance the photovoltaic performance, a method named Hot Solution Spin-coating (HSS) was used. In HSS method, a hot (60 °C) precursor solution (containing the more ratio of MACl/MABr /PbI₂ equal to 4:1:3) was quickly dropped on the spin coater and spin right away. Since the solution is still hot, solvent evaporates (or solution concentrated) quickly during the spinning and continuous film with no isolated grain was formed. SEM images displayed in Figure 4 reveal that the mixed-halide perovskite film prepared with HSS is very flat and the grain size is larger than that prepared from cold

precursor solution. The two λ_{max} of the UV/Vis absorption spectrum for HSS made film are close to those of the film made from cold precursor solution, indicating the stoichiometries of Br/I in both films are similar. Not so surprisingly, the inverted cell based on the film prepared by HSS method has the average efficiency up to 14% (see Table 3 and the I-V curve of the highest efficiency cell was illustrated in Figure S2, ESI).

Furthermore, we had shown previously¹⁹ that solvent annealing (SA) of the perovskite film with DMF can enlarge the grains size of the film (when the film is continuous without large hole) to enhance the photovoltaic performance. The same strategy was used to treat the mixed-halide film and the grain size increases further as the SEM images displayed in Figure 4. The inverted cell based on the film prepared by combining HSS and SA exhibited the efficiency more than 16% with high Voc of 1.1 V (see Table 3). The high-efficiency cells are very reproducible as the efficiency statistics data (based on 34 devices) shown in Figure S3, ESI. The high-efficiency cell also has no current hysteresis at two scan directions, various scan rates (see Figure S4 (a), ESI), the stable steady-state Jsc as a function of time is illustrated in Figure S4 (b), ESI and the current density integrated from the IPCE curve is very close to that measured from the I-V curve (see Figure S4 (c), ESI). We also used the same film preparation procedure to prepare full-iodide perovskite (MAPbI₃) film from the 0.35 M (MAI + PbI₂) precursor solution and the photovoltaic parameters of the corresponding cell are also listed in the bottom of Table 3. The efficiency of the inverted MAPbI₃ cell is less than 4%, due to the quick crystallization nature of the full-iodide lead perovskite. This is one of the reasons that mixed-halide perovskite was used to develop the simple film fabrication method.

To prepare perovskite film for the small area (typically 0.1 cm²) cells to reach high efficiency and good reproducibility have been achieved using several methods

such as two-step spin-coating,¹⁹ anti-solvent washing²⁶ and PbI₂ seeding⁴¹ by several research groups. However, up scaling these method to prepare large film for the solar module increases the complexity of the processing, therefore the efficiency of the module is in generally lower than that of the small cell.⁴² For example, Malinkiewicz⁴³ *et al.* compared the photovoltaic data of the large-area (1 cm²) cells with the standard-sized (0.09 cm²) cells and found that the conversion efficiency dropped from 12% for the small cells to 8.3% for the large ones. Most of the reduction in efficiency results from a decreasing in the fill factor. Thus developing a simple film preparation method is very important for scaling up the process to fabricate solar module for the practical applications. The one-step HSS + SA method we developed for fabricating high-quality mixed-halide perovskite film is very simple, reproducible and straightforward. Therefore it could be readily adopted to prepare large area perovskite film. The designed inverted perovskite solar module composes of 9 cells in series with the active area of each cell equal to 4 mm x 70 mm. The illustration of the ITO pattern on the substrate and the cross-section of the resulting perovskite solar module as well as the picture of the real device are displayed in Figure S5, ESI. The quality of the large-area perovskite film is almost as good as the small-area film as the SEM micrographs presented in Figure 5. The large-area perovskite film is very flat composed of big grains and having good attachment to PEDOT:PSS layer as the illustration of the cross-section image. The thickness of the film is *ca* 230 nm (from both SEM cross-section image and depth profile meter) which is also close to that of small area film prepared with the same precursor solution using the same method.

Figure 6 (a) shows the I-V characteristic of the inverted perovskite solar module based on the mixed-halide perovskite film prepared by using one-step HSS combined with SA method. The module exhibits a Voc of 9.05 V (average for each cell is 1.06 V), Isc of 53.5 mA, remarkable high FF of 0.744 and the overall conversion efficiency

of 14.3% which is the highest value of the perovskite solar module as our best knowledge. Moreover, perovskite solar module generally showed photocurrent hysteresis at different scan directions or scan rates.^{14,16} The photocurrent hysteresis of the module may be due to either the charge traps (so called capacity effect) on perovskite film with defects, unbalance in the electron and hole transport, ferroelectric properties of perovskite material and/or the migration of ion in perovskite. The $I-V$ curves for the module measured in different voltage scan directions reveal almost no photocurrent hysteresis, suggesting that the large area mixed-halide perovskite film prepared with the new method has a good quality: maybe as good as the small-area film. The same conclusion was derived from the SEM images shown in Figure 4 and Figure 5. To evaluate the film homogeneity more directly, light beam induced current (LBIC) mapping for the module was taken and illustrated in Figure 6 (b). The spatial map is obtained by illuminating the sample with a diode laser having wavelength of 530 nm. The related EQE values on LBIC map of the inverted solar module are quite uniform with no significant border effect. That is why the solar module (composed of 9 cells having the size of 4 mm x 70 mm arranged in series) exhibits so high power conversion efficiency. Nevertheless, the EQE inhomogeneity was still observed in the LBIC map displayed in Figure 6 (b). It may not just relate to the quality of the perovskite film, but also due to the properties of other components of the interphases of the module. More creative film preparation method and interphase engineering are needed to further improve the quality of the inverted perovskite solar module to increase the power conversion efficiency.

In conclusion, we had developed an one-step hot solution spin-coating method to prepare high quality mixed-halide perovskite films reproducibly. The advantage of using three types of halogens in the precursor solution is that Cl can improve the morphology of film by reducing the crystallization rate of perovskite and Br can

increase the V_{oc} of the corresponding device and stabilize the perovskite lattice. Therefore good quality film can be prepared using very simple one-step method to achieve high efficiency over 16%. The film fabrication method is so simple that it can be readily adopted to up scaling the film size for the inverted perovskite solar module to achieve high efficiency. Combining the halogens stoichiometry engineering, known solvent annealing and new developed HSS method, high quality, large-area mixed-halide perovskite film can be prepared and the corresponding inverted solar module achieve a record-high efficiency of 14.3% with remarkable high fill factor of 0.744. The study provides a big step toward fabricating low-cost perovskite solar modules for the commercial applications.

Experimental

Materials and Physicochemical Studies. Aqueous dispersion of PEDOT:PSS (1.3~1.7 wt%, from H.C. Stark Baytron P, AI 4083) was obtained from Heraeus Co. Fullerene derivatives PC₆₁BM (99.58%) were purchased from Solenne B. V., Netherlands. PbI₂ (99.999%) was bought from Aldrich Co. All materials were used as received except specified. ITO-covered glass substrates purchased from Ruilong optoelectronic Co., Taiwan were photolithographically patterned in our laboratory with HCl_(aq) for small area cell. The ITO pattern for the module was designed by us but fabricated by Ruilong Co. Taiwan. CH₃NH₃I, CH₃NH₃Br and CH₃NH₃Cl (MAI, MABr and MACl) were synthesized with the method similar to that reported in the literature.²³ Uv/Vis absorption spectra were recorded with a Hitachi F-7000 spectrometers. The thickness of the films was measured with a depth-profile meter (Veeco Dektak 150, USA). Five lines on the 1 cm x 1 cm film were made by carefully scratching with a tip and the average height between the hills and valleys is used to represent the film thickness. GIXRD data were collected in the 2 θ range 5 ~ 50 degree

on a Bruker powder diffractometer (D8 Discover) using Cu K α 1 radiation equipped with a 2D detector. Scanning Electron Micrograph (SEM) and Energy Dispersive Spectroscopy (EDS) data were obtained with a Hitachi S-800 microscopy at 15 KV. Samples (films on the substrate) for SEM surface and cross-section imaging and EDS study were mounted on a metal stub with a piece of conducting tape then coated with a thin layer of gold film to avoid charging. The cross-section image of the film was also used to estimate the thickness of perovskite.

Fabrication of the inverted perovskite solar cells and modules. PEDOT:PSS was spin-coated on a pre-patterned ITO glass at 5000 rpm for 50 sec and then annealed at 120°C for 10 min. For fabrication the mixed-halide perovskite (CH₃NH₃PbI_{3-x-y}Br_xCl_y) and full-iodide (CH₃NH₃PbI₃) film using one-step method, various amounts of PbI₂, CH₃NH₃I, CH₃NH₃Br and CH₃NH₃Cl were mixed and dissolved in DMF then stirred overnight in a glove box to make the precursor solutions. After passing the solution through a 0.22 μ m filter, perovskite film was formed by spin-coating the precursor solution on PEDOT:PSS coated ITO substrate using various spin rates and times. Specifically, in this study the highest efficiency device was based on CH₃NH₃PbI_{3-x-y}Br_xCl_y film fabricated from the precursor solution containing PbI₂, MABr, MACl in the mole ratio of equal to 3:1:4 and the concentration of PbI₂ is 0.35 M. The spin program is 1000 rpm for 10 seconds then 7000 rpm for 20 seconds. For the hot solution spin-coating (HSS), the filtered precursor solution was heated to 60°C then dropped on the substrate and spin right away. After perovskite film was annealed at 100°C for 10 min, 2 wt% PCBM in chlorobenzene was spin-coated onto perovskite layer at 1500 rpm for 30 sec. The solvent annealing (SA) was carried out by covering the film with DMF together at room temperature for 24 hours after perovskite film was heated at 100°C for 10 min. The PEDOT:PSS/perovskite/PCBM film was transferred to a vacuum chamber for

coating Ca/Al electrode (20 nm/100 nm) to obtain the inverted perovskite solar cell. All the fabrication procedures except the deposition of PEDOT:PSS layer were carried out in a N₂-filled glove box. The active area of the cell is 0.5 cm x 0.2 cm. The films made from the same batch of the precursor solution were used to synthesize perovskite films for EDS/SEM, GIXRD and Uv/Vis measurements as well as for fabricating solar cell. The process for fabricating solar module is very similar to that used for assembling small cell except the pre-patterned large area ITO electrode was used and large amount of the PEDOT:PSS aqueous suspension, hot (60°C) precursor solutions and PCBM solution were applied on the substrate in the spin-coating process. The active area of the module is 25.2 cm² (mask area) by connecting 9 cells in series (the active area of each cell is 4 mm x 70 mm).

The photovoltaic performance and light beam induced current (LBIC) measurements. The solar cell and module were covered with a defined mask. The *I-V* characteristics of the cells were measured using a Keithley 4200 source measuring unit under a simulated AM 1.5G light (Wacom solar simulator for the cells and Yamashita solar simulator for the modules) at 100 mWcm⁻² and the light intensity was calibrated by KG-5 Si diode. External quantum efficiency (EQE) or incident photo-to-current conversion efficiency (IPCE) was measured in air after sealing the device with a silica sealant and measured immediately. A chopper and lock-in amplifier were used for the phase sensitive detection with QE-R3011 measurement system (Enlitech Inc., Taiwan). The LBIC system used in this study was designed also by Enlitech Inc., Taiwan. The light for LBIC (or called spatially resolved photocurrent map) measurement is provided by a green laser diode with the wavelength of 530 nm which matches the absorption region of the perovskite solar cells. The intensity of the light was first calibrated by a silicon diode and the module was fixed on an x-y motorized stage. The scanning step of the stage is 0.5 mm and the diameter of the laser

light beam is 10 μm . The intensity of the laser light was measured before and after the sample measurements to ensure that the light intensity of the laser is very stable. It takes *ca.* 10 hours to finish one LBIC measurement. The photocurrent (equal to EQE) produced on each point can be used as an indication for the homogeneity (quality) of each layer and the interphases of the perovskite solar module. The determination of the photovoltaic parameters and the calibration of all measuring facilities are the same as what we reported previously.¹⁹

Acknowledgements

Financial support from the Ministry of Science and Technology (MOST), Taiwan, ROC (grand number: NSC101-2113-M-008-008-MY3) is gratefully acknowledged. The devices fabrication was carried out in Advanced Laboratory of Accommodation and Research for Organic Photovoltaics, MOST, Taiwan, ROC.

Supporting Information Available:

Supplementary data are collected in the Electronic Supporting Information (ESI). This material is available online with the article.

References:

1. A. Kojima, K. Teshima, Y. Shirai, T. Miyasaka, *J. Am. Chem. Soc.*, 2009, **131**, 6050-6051.
2. H. Zhou, Q. Chen, G. Li, S. Luo, T.-B. Song, H.-S. Duan, Z. Hong, J. You, Y. Liu, Y. Yang, *Science*, 2014, **345**, 542-546.
3. J. You, Z. Hong, Y. (M.) Yang, Q. Chen, M. Cai, T.-B. Song, C.-C. Chen, S. Lu, Y. Liu, H. Zhou, Y. Yang, *ACS Nano*, 2014, **8**, 1674-1680.
4. Y. Zhao, K. Zhu, *J. Am. Chem. Soc.*, 2014, **136**, 12241-12244.
5. National Renewable Energy Laboratory, Best Research Cell Efficiency. (http://www.nrel.gov/ncpv/images/efficiency_chart.jpg).
6. D. B. Mitzi, S. Wang, C. A. Feild, C. A. Chess, A. M. Guloy, *Science*, 1995, **267**, 1473-1476.
7. H.-S. Kim, C.-R. Lee, J.-H. Im, K.-B. Lee, T. Moehl, A. Marchioro, S.-J. Moon, R. Humphry-Baker, J.-H. Yum, J. E. Moser, M. Grätzel, N.-G. Park, *Scientific Reports*, 2012, **2**, 591-597
8. J. Burschka, N. Pellet, S.-J. Moon, R. Humphry-Baker, P. Gao, M. K. Nazeeruddin, M. Grätzel, *Nature*, 2013, **499**, 316-319.
9. M. Liu, M. B. Johnston, H. J. Snaith, *Nature*, 2013, **501**, 395-398.
10. C. Kagan, D. Mitzi, C. Dimitrakopoulos, *Science*, 1999, **286**, 945-947.
11. H. Zhou, Q. Chen, G. Li, S. Luo, T. Song, S.-H. Duan, Z. Hong, J. You, Y. Liu, Y. Yang, *Science*, 2014, **345**, 542-546.
12. G. E. Eperon, V. M. Burlakov, P. Docampo, A. Goriely, H. J. Snaith, *Adv. Funct. Mater.*, 2014, **24**, 151-157.
13. Q. Chen, H. Zhou, Z. Hong, S. Luo, H.-S. Duan, H.-H. Wang, Y. Liu, G. Li, Y. Yang, *J. Am. Chem. Soc.*, 2014, **136**, 622-625.
14. Q. Guo, C. Li, W. Qiao, S. Ma, F. Wang, B. Zhang, L. Hu, S. Dai, Z. Tan, *Energy Environ. Sci.*, 2016, 10.1039/c5ee03620h);

15. S. Razza, F. Di Giacomo, F. Matteocci, L. Cina, A. L. Palma, S. Casaluci, P. Cameron, A., D'Epifanio, S. Licoccia, A. Reale, T. M. Brown, A. Di Carlo, *J. Power Sources*, 2015, **277**, 286-291.
16. W., Qiu, T. Merckx, M. Jaysankar, C. M. de la Huerta, L. Rakocevic, W. Zhang, U. W. Paetzold, R. Gehlhaar, L. Froyen, J. Poortmans, D. Cheyns, H. J. Snaith, P. Heremans, *Energy Environ. Sci.*, 2016, **9**, 484-489.
17. J. H. Heo, H. J. Han, D. Kim, T. K. Ahn, S. H. Im, *Energy Environ. Sci.*, 2015, **8**, 1602-1608.
18. C. H. Chiang, Z. L. Tseng, C. G. Wu, *J. Mater. Chem. A*, 2014, **9**, 15897-15903.
19. C. G. Wu, C. H. Chiang, Z. L. Tseng, K. M. Nazeeruddin, A. Hagfeldt, M. Grätzel, *Energy Environ. Sci.*, 2015, **8**, 2725-2733.
20. C. G. Wu, C. H. Chiang, S. H. Chang, *Nanoscale*, 2016, **8**, 4077-4082.
21. E. Mosconi, A. Amat, Md. K. Nazeeruddin, M. Grätzel, F. De Angelis, *J. Phys. Chem. C*, 2013, **117**, 13902-13913.
22. M. M. Lee, J. I. Teuscher, T. Miyasaka, T. N. Murakami, H. J. Snaith, *Science*, 2012, **338**, 643-647.
23. L. Etgar, P. Gao, Z. Xue, Q. Peng, A. K. Chandiran, B. Liu, M. K. Nazeeruddin, M. Grätzel, *J. Am. Chem. Soc.*, 2012, **134**, 17396-17399.
24. Z. Cheng, J. Lin, *CrystEngComm.*, 2010, **12**, 2646-2662.
25. J. H. Noh, S. H. Im, J. H. Heo, T. N. Mandal, S. I. Seok, *Nano Lett.*, 2013, **13**, 1764-1769.
26. N. J. Jeon, J. H. Noh, Y. C. Kim, W. S. Yang, S. Ryu, S. I. Seok, *Nat. Mater.*, 2014, **13**, 897-903.
27. G. Xing, N. Mathews, S. Sun, S. S. Lim, Y. M. Lam, M. Gratzel, S. Mhaisalkar, T. C. Sum, *Science*, 2013, **342**, 344-347.
28. J. H. Heo, D. H. Song, S. K. Im, *Adv. Mater.*, 2014, **26**, 8179-8183.

29. S. Ryu, J. H. Noh, N. J. Jeon, Y. C. Kim, W. S. Yang, J. Seo, S. I. Seok, *Energy Environ. Sci.*, 2014, **7**, 2614-2618.
30. Y. Zhao, K. Zhu, *J. Am. Chem. Soc.*, 2014, **136**, 12241-12244.
31. W. Nie, H. Tsai, R. Asadpour, J.-C. Blancon, A. J. Neukirch, G. Gupta, J. J. Crochet, M. Chhowalla, S. Tretiak, M. A. Alam, H.-L. Wang, A. D. Mohite, *Science*, 2015, **347**, 522-525.
32. J. W. Jung, S. T. Williamsa, A. K.-Y. Jen, *RSC Adv.*, 2014, **4**, 62971-62977.
33. E. Mosconi, E. Ronca, F. D. Angelis, *J. Phys. Chem. Lett.*, 2014, **5**, 2619.
34. P. Dokurno, J. Łubkowski, J. Błażejowski, *Thermochim. Acta.*, 1990, **165**, 31-48.
35. H. J. Snaith, A. Abate, J. M. Ball, T. Leijtens, N. K. Noel, S. D. Stranks, J. T. Wang, K. Wojciechowski, W. Zhang, *J. Phys. Chem. Lett.*, 2014, **5**, 1511-1515.
36. T. Leijtens, J. Lim, J. Teuscher, T. Park, H. J. Snaith, *Adv. Mater.*, 2013, **25**, 3227-3233.
37. J.-H. Im, C.-R. Lee, J.-W. Lee, S.-W. Park, N.-G. Park, *Nanoscale*, 2011, **3**, 4088-4093.
38. B. Conings, L. Baeten, C. De Dobbelaere, J. D'Haen, J. Manca, H.-G. Boyen, *Adv. Mater.*, 2014, **26**, 2041-2046.
39. E. Edri, S. Kirmayer, D. Cahen, G. Hodes, *J. Phys. Chem. Lett.*, 2013, **4**, 897-902.
40. A. Poglitsch, D. Weber, *J. Chem. Phys.*, 1987, **87**, 6373-6378.
41. Z. Xiao, C. Bi, Y. Shao, Q. Dong, Q. Wang, Y. Yuan, C. Wang, Y. Gao, J. Huang, *Energy Environ. Sci.*, 2014, **7**, 2619-2623.
42. W. Qiu, T. Merckx, M. Jaysankar, C. Masse de la Huerta, L. Rakocevic, W. Zhang, U. W. Paetzold, R. Gehlhaar, L. Froyen, J. Poortmans, D. Cheyns, H. J. Snaith, P. Heremans, *Energy Environ. Sci.*, 2016, **9**, 484-489.
43. O. Malinkiewicz, A. Yella, Y. H. Lee, G. M. Espallargas, M. Graetzel, M. K. Nazeeruddin, H. J. Bolink, *Nature Photon.*, 2014, **8**, 128-132.

Figure caption:

Figure 1: GIXRD patterns of $\text{CH}_3\text{NH}_3\text{PbI}_{2.4}\text{Cl}_{0.6}$ (Film-1), $\text{CH}_3\text{NH}_3\text{PbI}_{2.2}\text{Br}_{0.3}\text{Cl}_{0.5}$ (Film-2) and $\text{CH}_3\text{NH}_3\text{PbI}_{2.09}\text{Br}_{0.65}\text{Cl}_{0.26}$ (Film-3) (the signals at 2θ of $10 \sim 16^\circ$ and $27 \sim 31^\circ$ were enlarged for showing the shift of the diffraction peaks).

Figure 2: UV/Vis absorption spectra of $\text{CH}_3\text{NH}_3\text{PbI}_3$, $\text{CH}_3\text{NH}_3\text{PbI}_{2.4}\text{Cl}_{0.6}$ (Film-1), $\text{CH}_3\text{NH}_3\text{PbI}_{2.2}\text{Br}_{0.3}\text{Cl}_{0.5}$ (Film-2) and $\text{CH}_3\text{NH}_3\text{PbI}_{2.09}\text{Br}_{0.65}\text{Cl}_{0.26}$ (Film-3).

Figure 3: SEM images of (a) $\text{CH}_3\text{NH}_3\text{PbI}_{2.4}\text{Cl}_{0.6}$ (Film-1), (b) $\text{CH}_3\text{NH}_3\text{PbI}_{2.2}\text{Br}_{0.3}\text{Cl}_{0.5}$ (Film-2) and (c) $\text{CH}_3\text{NH}_3\text{PbI}_{2.09}\text{Br}_{0.65}\text{Cl}_{0.26}$ (Film-3).

Top: low magnification; middle: high magnification; bottom: cross-section.
(The concentration of PbI_2 in the precursor solutions is 0.6 M)

Figure 4: SEM images of the mixed-halide perovskite film prepared with (a) cold solution spin-coating method (b) hot solution spin-coating (HSS) method (c) combining HSS and solvent annealing (SA) methods.

(Top: low magnification; bottom: high magnification)

Figure 5: SEM images (surface (left) and cross-section(right)) of the large-area mixed-halide perovskite film prepared by combining HSS and SA method.

Figure 6: (a) I-V curve (b) LBIC map of the mixed-halide perovskite solar module (containing 9 cells (with 4 mm x 70 mm for each cell) in series).

Table 1: The photovoltaic performance of perovskite films fabricated with one-step method from the precursor solutions containing various amount of halides.

^a Mole ratio of MAI:MABr:MAI:PbI ₂ in precursor solution	<i>J</i> _{sc} (mA/cm ²)	<i>V</i> _{oc} (V)	<i>FF</i>	η (%)	Code of the film
^b 0:0:1:1	7.86	0.64	0.52	2.62	Film-0
4:0:0:3	12.7	0.91	0.45	5.20	Film-1
4:1:0:3	14.96	1.00	0.62	9.28	Film-2
4:2:0:3	12.6	1.02	0.53	6.81	Film-3
4:3:0:3	3.29	0.59	0.29	0.563	Film-4
3:1:0:3	9.10	0.32	0.31	0.903	Film-5
6:1:0:3	9.20	0.84	0.41	3.17	Film-6
5:1:0:3	8.22	0.91	0.43	3.22	Film-7

a. Concentration of PbI₂ is 0.6 M. Spin program for depositing perovskite film: 5000 rpm, 30 sec..

b. The precursor solution for preparing full-iodide (CH₃NH₃PbI₃) perovskite film.

Table 2: The stoichiometry of the halogen atoms in the precursor solutions and the resulting films.

Atomic ratio of Cl : Br : I in the precursor solution	Atomic ratio of Cl : Br : I in the resulting film	d-spacing (Å)	Code of the film
4 : 0 : 6	$\text{CH}_3\text{NH}_3\text{PbI}_{2.4}\text{Cl}_{0.6}$	6.43	Film-1
4 : 1 : 6	$\text{CH}_3\text{NH}_3\text{PbI}_{2.2}\text{Br}_{0.3}\text{Cl}_{0.5}$	6.38	Film-2
4 : 2 : 6	$\text{CH}_3\text{NH}_3\text{PbI}_{2.09}\text{Br}_{0.65}\text{Cl}_{0.26}$	6.32	Film-3
---	$\text{CH}_3\text{NH}_3\text{PbI}_3$	6.43	MAPbI₃
---	$\text{CH}_3\text{NH}_3\text{PbBr}_3$	5.83	MAPbBr₃

Concentration of PbI_2 is 0.6 M.

Spin program: 5000 rpm for 30 sec.

Table 3: The photovoltaic performance of the mixed-halide perovskite film fabricated from various precursor concentrations and spin programs using one-step method.

^a PbI ₂ concentration	Spin rate (rpm)	<i>J</i> _{sc} (mA/cm ²)	<i>V</i> _{oc} (V)	<i>FF</i>	Highest η (%) (average η)
0.7	5000	15.27	0.98	0.491	7.34
0.6	5000	14.96	1.00	0.624	9.34
0.3	5000	7.33	0.46	0.284	1.12
0.35	1000	11.4	0.20	0.258	0.87
0.35	3000	12.8	0.27	0.291	1.26
0.35	^b 1000, 5000	14.3	0.970	0.664	9.04
0.35	1000, 7000	15.23	1.03	0.75	11.77 ^c (10.29±0.78)
0.35	1000, 8000	15.40	0.89	0.66	9.05
^d HSS		18.31	1.04	0.76	14.47 ^c (14.04 ± 0.75)
^e HSS + SA		19.25	1.10	0.78	16.52 ^f (15.61 ± 0.84)
^g HSS + SA (MAPbI ₃)		10.29	0.90	0.39	3.61

- a. The mole ratio of MAI:MABr:PbI₂ is 4:1:3.
- b. 1000, 5000 means 1000 rpm for 10 sec. and then 5000 rpm for 20 sec.
- c. The device performance statistics is based on 21 devices.
- d. HSS: Hot Solution Spin-coating using the spin program of 1000 rpm for 10 sec. and then 7000 rpm for 20 sec.
- e. HSS (as d) combining with Solvent Annealing (SA).
- f. The device performance statistics is based on 34 devices.
- g. The active absorber is full iodide perovskite (MAPbI₃).

One-step Fabrication of Mixed-Halide Perovskite Film for High-efficiency Inverted Solar cell and Module

Chien-Hung Chiang^b, Jun-Wei Lin^a, Chun-Guey Wu^{a,b,*}

* ^{a,b} Professor: Chun Guey Wu, Master student: Chun-Wei Lin,
Department of Chemistry and Research Center for New Generation Photovoltaics,
National Central University, Jhong-Li, Taiwan 32001, ROC.
Fax: 886-3-4227664
E-mail: t610002@cc.ncu.edu.tw.

^b Research associate: Chien-Hung Chiang
Research Center for New Generation Photovoltaics,
National Central University, Jhong-Li, Taiwan 32001, ROC.

Figure 1:

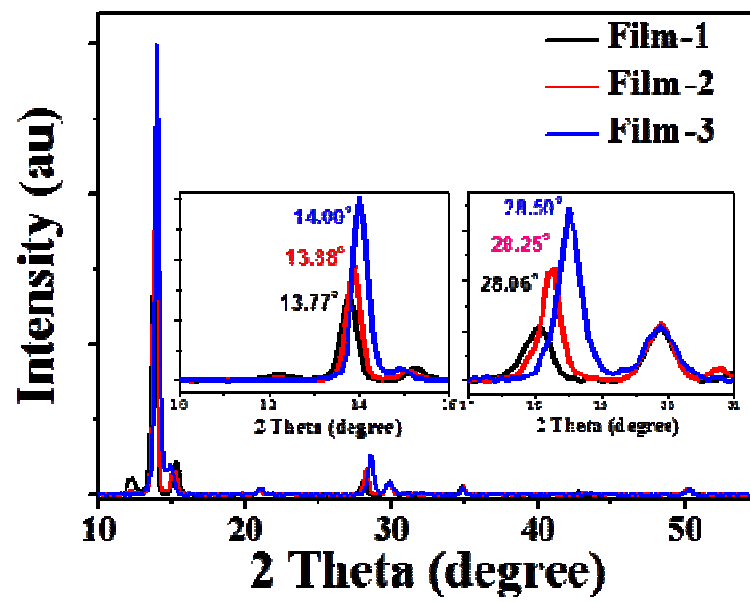


Figure 2:

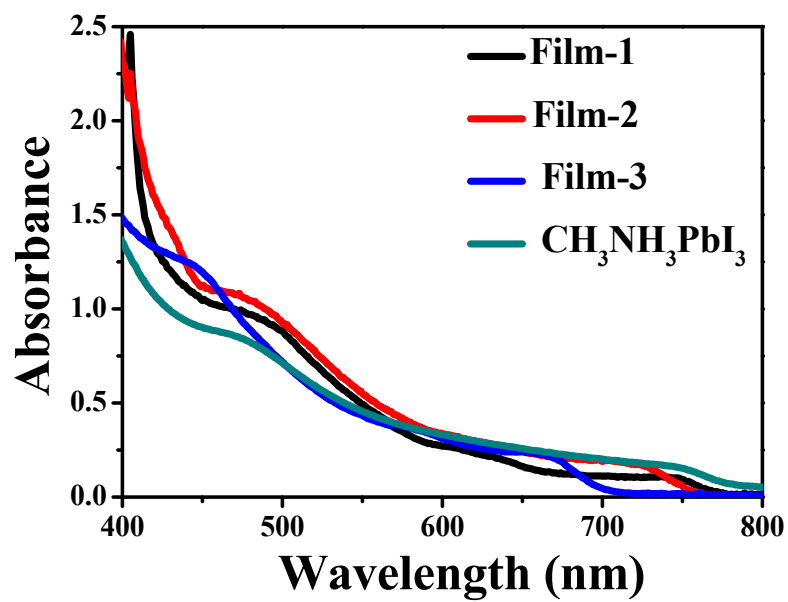


Figure 3

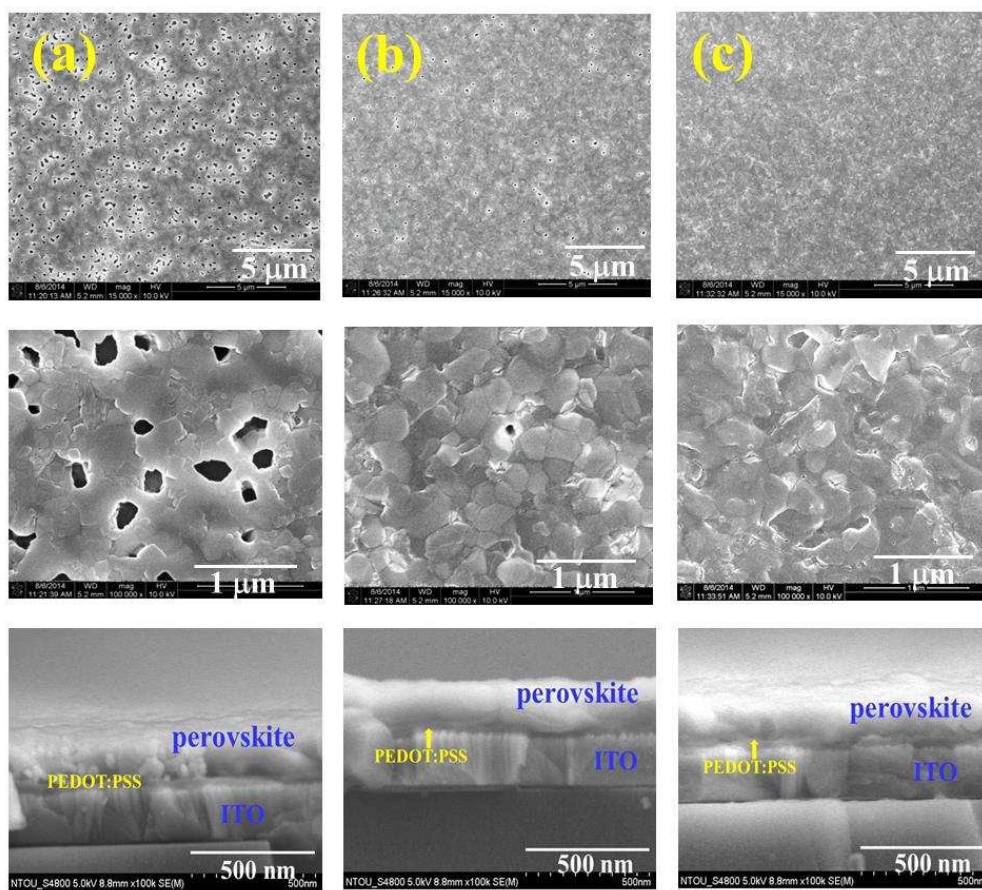


Figure 4:

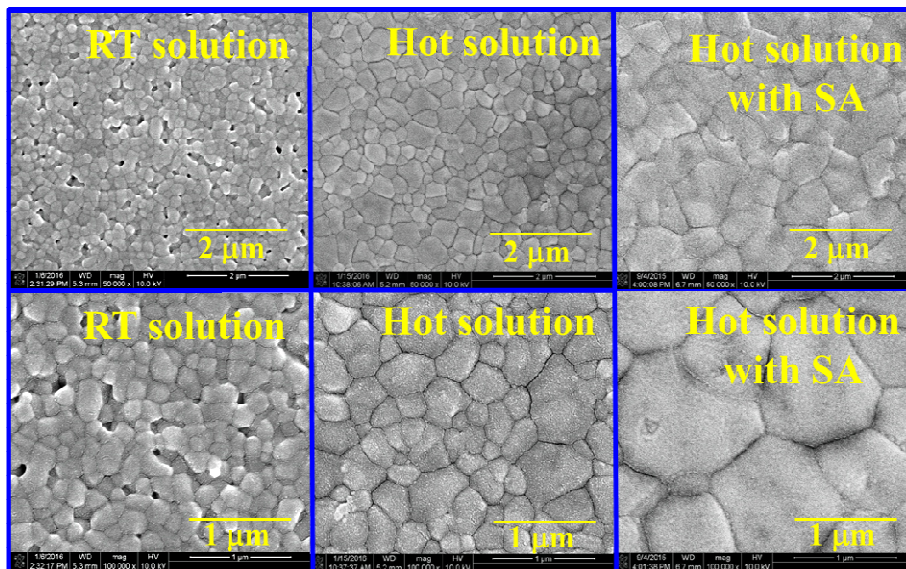


Figure 5

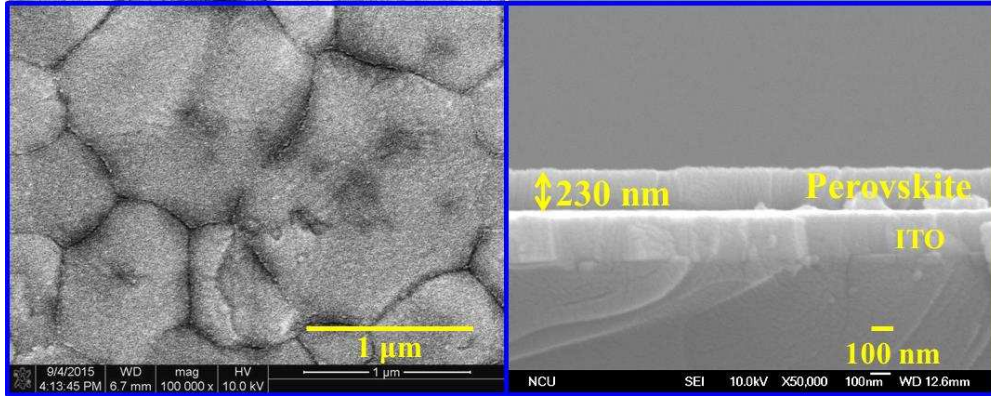
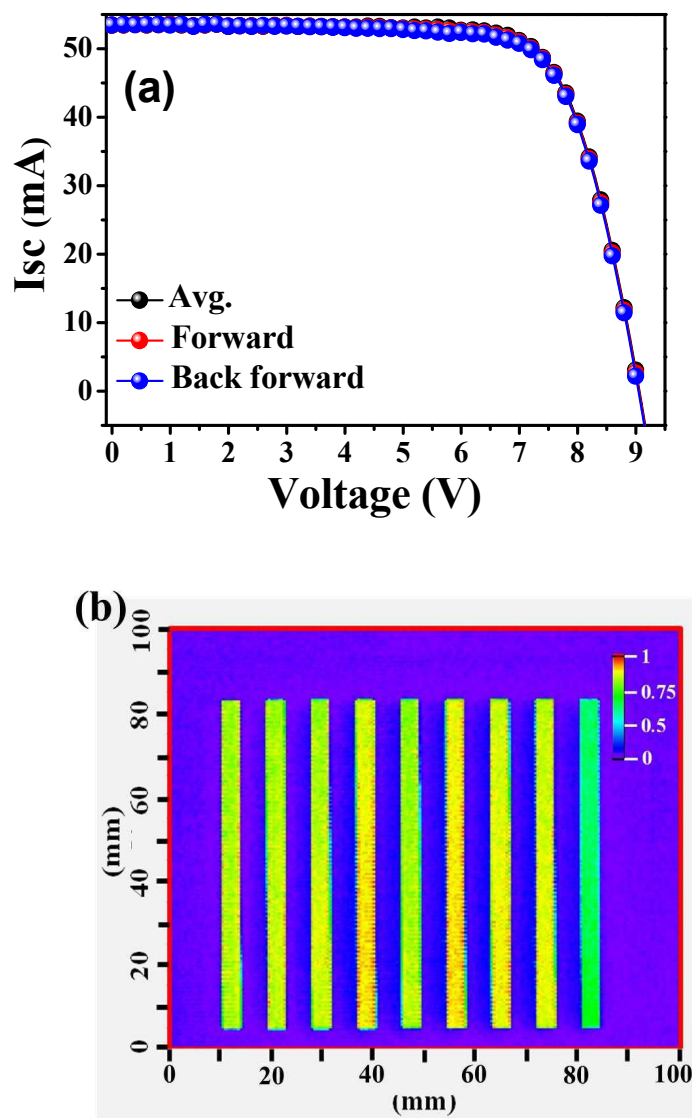
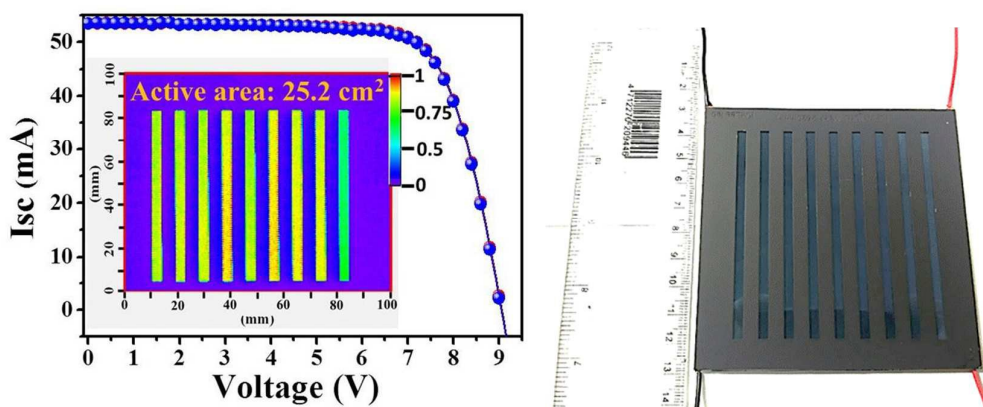


Figure 6



Graphical table of content

Combination the halogens composition and film casting engineering, large area, good quality and homogeneous film can be prepared with a real one-step method (no anti-solvent). Inverted solar cell (0.1 cm²) and module (active area of 25.2 cm²) based on the mixed-halide perovskite films achieve the highest efficiency of 16.52% and 14.3%, respectively.